

A model of random center vortex lines in continuous 2+1-dimensional space-time

Derar Altarawneh,^{1,*} Michael Engelhardt,^{2,†} and Roman Höllwieser^{c2,3,§}

¹*Department of Applied Physics, Tafila Technical University, Tafila , 66110 , Jordan*

²*Department of Physics, New Mexico State University,*

PO Box 30001, Las Cruces, NM 88003-8001, USA

³*Institute of Atomic and Subatomic Physics, Vienna University of Technology, Operngasse 9, 1040 Vienna, Austria*

(Dated: June 24, 2016)

A picture of confinement in QCD based on a condensate of thick vortices with fluxes in the center of the gauge group (center vortices) is studied. Previous concrete model realizations of this picture utilized a hypercubic space-time scaffolding, which, together with many advantages, also has some disadvantages, e.g., in the treatment of vortex topological charge. In the present work, we explore a center vortex model which does not rely on such a scaffolding. Vortices are represented by closed random lines in continuous 2+1-dimensional space-time. These random lines are modeled as being piece-wise linear, and an ensemble is generated by Monte Carlo methods. The physical space in which the vortex lines are defined is a torus with periodic boundary conditions. Besides moving, growing and shrinking of the vortex configurations, also reconnections are allowed. Our ensemble therefore contains not a fixed, but a variable number of closed vortex lines. This is expected to be important for realizing the deconfining phase transition. We study both vortex percolation and the potential $V(R)$ between quark and anti-quark as a function of distance R at different vortex densities, vortex segment lengths, reconnection conditions and at different temperatures. We find three deconfinement phase transitions, as a function of density, as a function of vortex segment length, and as a function of temperature.

PACS numbers: 11.15.Ha, 12.38.Gc

Keywords: Center Vortices, Quark Confinement

CONTENTS

I. Introduction	2
II. The Model	3
A. Move, Add & Delete	3
B. Reconnections	5
C. Parameters	5
D. Monte Carlo Algorithm	6
III. Observables	6
A. Vortex Cluster Analysis	6
B. Wilson Loops	7
IV. Results & Discussion	7
A. Finite temperature phase transition from varying temporal extent L_T	7
B. Deconfining transition as a function of vortex density cutoff d	10
C. Phase transition from varying maximal vortex length L_{max}	10
D. Behavior as a function of minimal vortex/reconnection length L_{min}	13
V. Conclusions & Outlook	15
Acknowledgments	17
References	17

^c Funded by an Erwin Schrödinger Fellowship of the Austrian Science Fund under Contract No. J3425-N27.

^{*} derar@ttu.edu.jo

[†] engel@nmsu.edu

[§] hroman@kph.tuwien.ac.at

I. INTRODUCTION

Quantum Chromodynamics (QCD) is the regnant theory of the strong interaction. It is formulated in terms of quarks and gluons, which are the basic degrees of freedom that make up hadronic matter. QCD is well understood in the regime where we have a large momentum transfer (ultraviolet regime). In this regime, the theory is weakly coupled and can thus be solved using perturbative methods. On the other hand, at low energy, analytical solutions are very hard to obtain due to the large coupling constant and the highly nonlinear nature of the strong force. It happens especially in this infrared regime that the QCD vacuum exhibits some extraordinary features, among them the confinement of quarks into bound hadrons and chiral symmetry breaking (χ SB), the origin of mass in QCD. A perspective to construct a cogent, comprehensive model of the strong interaction vacuum in which, in particular, a connection between topological properties and confinement can be drawn, appeared in the framework of the magnetic (center) vortex picture [1–6]: Chromo-magnetic flux lines compress the chromo-electric flux between color electric sources into a flux tube (or a "string"), resulting in a linearly rising potential and thus confinement.

In D -dimensional space-time, center vortices are (thickened) $(D - 2)$ -dimensional chromo-magnetic flux degrees of freedom. The center vortex picture of the strong interaction vacuum assumes that these are the relevant degrees of freedom in the infrared sector of the strong interaction; the center vortices consequently are taken to be weakly coupled and can thus be expected to behave as random lines (for $D = 3$) or random surfaces (for $D = 4$). The magnetic flux carried by the vortices is quantized in units which are singled out by the topology of the gauge group, such that the flux is stable against small local fluctuations of the gauge fields. In the vortex model of confinement, the deconfinement transition results from a percolation transition of these chromo-magnetic flux degrees of freedom. This theoretically appealing picture has been buttressed by a multitude of numerical calculations, both in lattice Yang-Mills theory and within a corresponding infrared effective model, see *e.g.* [7–18], or [19], which summarizes the main features. Recent results [20] have also suggested that the center vortex model of confinement is more consistent with lattice results than other currently available models. Lattice studies further indicate that vortices may also be responsible for topological charge [21–29] and χ SB [30–43], and thus unify all non-perturbative phenomena engendered by the structure of the strong interaction vacuum in a common framework.

A concrete implementation of the vortex picture, using a hypercubic lattice scaffolding to support the random vortex lines or surfaces, has been studied extensively by one of the authors [12, 15, 22, 23, 34, 44–47]. The hypercubic formulation has a number of advantages, among them, simple Monte Carlo updates which naturally include surfaces fusing and disassociating, and a straightforward bookkeeping of vortex location, permitting, *e.g.*, simple evaluation of Wilson loops and counting of vortex surface intersections. On the other hand, however, this formulation has revealed weaknesses as far as the calculation of topological charge is concerned. Vortex world-surface configurations in this formulation, being restricted to only six discrete space-time directions in which they can extend, exhibit ambiguities in the definition of topological charge which would not appear in ensembles of arbitrary two-dimensional surfaces in continuous four-dimensional space-time.

In view of this, we explore in the present work an alternative formulation, which avoids the shortcomings of the hypercubic construction, concentrating in a first step on a model of random flux lines in $D = 2 + 1$ space-time dimensions, representing vortices of the $SU(2)$ gauge group (i.e., there are no branchings of the vortex lines [12, 15]). The lines are composed of straight segments connecting nodes randomly distributed in three-dimensional space. Allowance is made for nodes moving as well as being added or deleted from the configurations during Monte Carlo updates. Furthermore, Monte Carlo updates disconnecting and fusing vortex lines, *i.e.*, reconnection updates are implemented. Given that the deconfining phase transition is a percolation transition, such processes play a crucial role in the vortex picture. The model is formulated in a toroidal finite volume, with periodic boundary conditions, which allows for a study of finite temperatures (via changes in the temporal extent of the volume). The resulting vortex ensemble is used, in particular, to evaluate the string tension and its behavior as a function of temperature, with a view towards detecting the high-temperature deconfining phase transition.

The above scheme of modeling random lines (and higher-dimensional manifolds) is reminiscent of models employed in the study of quantum gravity [48–53]. While the present work focuses only on the lowest-dimensional case, the inclusion of a variable number of (vortex) clusters in the ensemble is a feature that is not generally contemplated in quantum gravity applications. Here, it is crucial in order to include the physics of the deconfinement transition. Also the use of a torus with periodic boundary conditions, on which the vortices are defined, in order to treat finite temperature, constitutes a significant complication.

This paper is organized as follows: The modeling details will be given in section II, observables will be introduced in section III, and results will be presented and discussed in section IV. Section V provides a summary of the main results and a short outlook.

II. THE MODEL

In the model, vortices are represented by closed random lines in 2+1-dimensional (Euclidean) space-time. The physical space in which the vortex lines are defined is a torus $L_S^2 \times L_T$ with "spatial" extent L_S , "temporal" extent L_T and periodic boundary conditions in all directions. The random lines are modeled as being piece-wise linear between "nodes" with vortex segment length L restricted to a certain range $L_{min} < L < L_{max}$. This range sets a scale of the model; for practical reasons we choose a scale of $L \approx 1$, *i.e.* $L_{min} = 0.3$ and $L_{max} = 1.7$ in appropriate units. Within this paper we use volumes with $L_S = 16$, where finite size effects are under control, and varying time lengths L_T . Variations of the vortex segment length range away from the aforementioned range will also be examined. An ensemble is generated by Monte Carlo methods, starting with a random initial configuration. A Metropolis algorithm is applied to add, move and delete nodes using the action

$$S = \alpha L + \gamma \varphi^2, \quad (1)$$

with action parameters α and γ for the vortex segment length L and the vortex angle φ at nodes, respectively. At a given (current) node the vortex segment length L is defined to be the distance to the previous node and the vortex angle is the angle between the oriented vectors of the vortex lines connecting the previous, current and next nodes, see Fig. 1. This type of action, penalizing both vortex length and curvature, is analogous to the action used in previous hypercubic lattice models [12, 15]. Furthermore, when two vortices approach each other, they can reconnect or separate at a bottleneck, as described in detail further below. The ensemble therefore will contain not a fixed, but a variable number of closed vortex lines or "vortex clusters". This is expected to be important for realizing the deconfining phase transition. Moreover, new (three-node) clusters are permitted to "pop out" of the vacuum at random positions, again governed by the above action; hence a small equilateral triangle is more probable than a long acute triangle, see Fig. 1. The new cluster then evolves further in subsequent updates, along with all other clusters. Also the reverse process, annihilation of a three-node cluster, is possible; it occurs when a node is deleted from a three-node cluster, leading to a two-node cluster. Such a cluster is equivalent to the absence of any flux, and is therefore deleted completely.

In the following, we discuss the individual updates and parameters of the model in more detail.

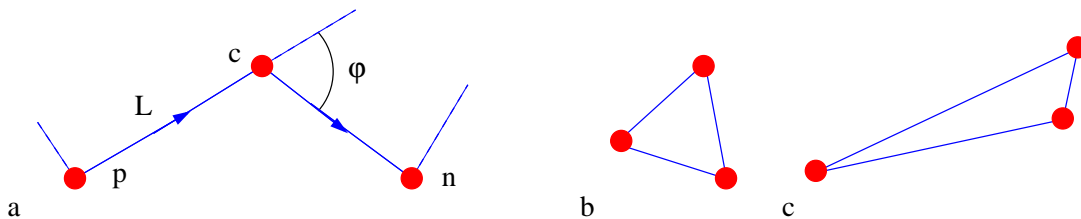


FIG. 1. a) The action $S = \alpha L + \gamma \varphi^2$ of the current node (c) is given by the vortex length L to the previous node (p) and the angle φ between the vortex lines to the previous (p) and the next node (n). Three node clusters of shape (b) are more likely accepted by the Metropolis algorithm than of shape (c).

A. Move, Add & Delete

Move, add and delete updates are applied to the vortex nodes via the Metropolis algorithm, *i.e.*, the difference of the action of the affected nodes before (S_i) and after (S_f) the update determines the probability $P = \min(1, \exp(S_i - S_f))$ of the update being accepted. The move update attempts to move the current node by a random vector of maximal length $r_m = 4L_{min}$; it affects the action of three nodes, the current node itself and its neighbors, see Fig. 2.

The add update attempts to add a node at a random position within a radius $r_a = 3L_{min}$ around the midpoint between the current and the next node, see Fig. 3. The action S_i before the update is given by the sum of the action at the current and the next node, while the action S_f after the update is the sum of the action at the current, the new and the next node. Conversely, deleting the current node affects three nodes, *i.e.* the previous, the current and the next node before the update and only two nodes (previous and next) after the update, see Fig. 4. Therefore the probability P for the add update is in general much smaller than for the delete update; the vortex structure tends to vanish quickly if both updates are tried equally often. As detailed below, add updates were attempted at a significantly larger rate than delete updates.

In general, move, add and delete updates can come into conflict with the restricted range of allowed vortex segment lengths L . In early implementations, the move update was applied to every node of the configuration, and if the

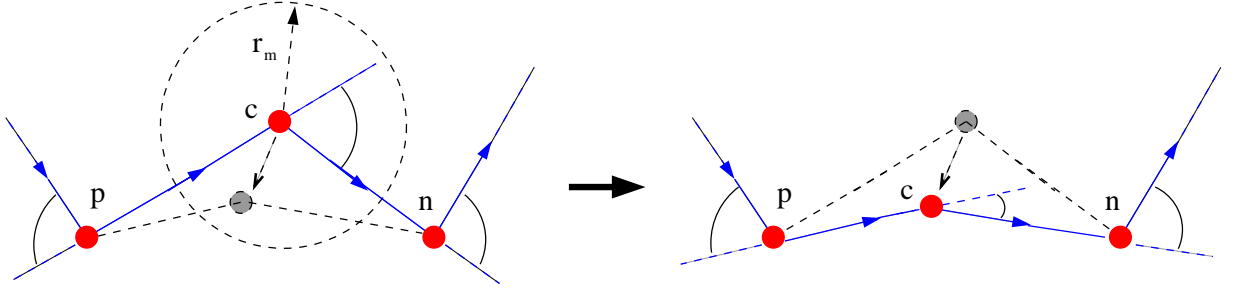


FIG. 2. The movement of the current node (c) within a certain range r_m is affecting the connected vortex lines and the angles at the current (c), the previous (p) and the next node (n).

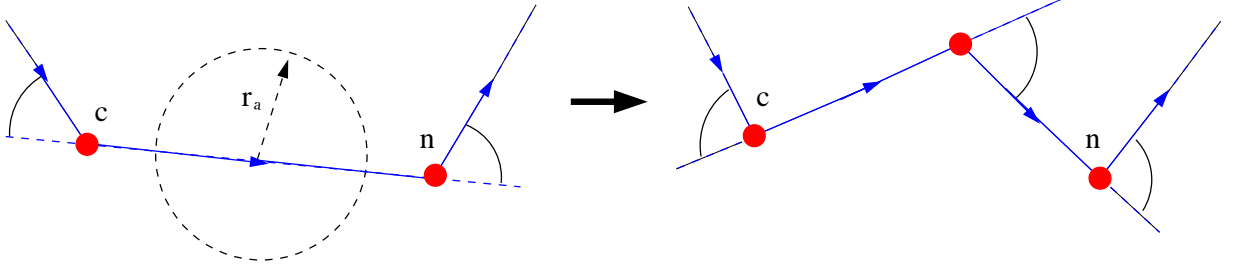


FIG. 3. The add update adds a node after the current node (c) within a range r_a around the midpoint of the vortex line to the next node (n). Two vortex angles before and three after the update are affected, and one vortex line is split into two.

resulting vortex segment lengths conflicted with the allowed range, the corresponding nodes were deleted, or auxiliary ones at midpoints were added, respectively. In principle, in this scheme, the configuration can be stabilized for a set of fine-tuned parameters, but these parameters lead to very dense vortex configurations deep in the confinement phase. Hence, in order to explore the whole phase space of the model, an additional density parameter d is introduced, restricting the number of nodes in a certain volume. The add update is rejected if the number of nodes within a $3 \times 3 \times 3$ volume around the new node exceeds the density parameter d . Also new clusters popping up are subjected to this density cutoff, *i.e.*, the number of nodes in a $3 \times 3 \times 3$ volume has to be less than $d - 3$ for a three-node cluster to pop up there. Further, all updates resulting in vortex segment lengths L out of the range $L_{min} < L < L_{max}$ are also rejected. The update strategy is randomized to move a node in two out of three cases (66%), and apply the add update about five times more often than the delete update (28% vs. 6%). Maximal movement and add "radii" r_m and r_a are set to four resp. three times L_{min} . The different parameters and restrictions in the model may seem artificial at first sight, but they are optimized in order to guarantee a balance between action and entropy of the system. The influence of the individual parameters on the model and their "physical" effect to favor either action or entropy will be discussed in Sec. IV. An overview of all parameters and the Monte Carlo sweep will be given in sections II C and II D respectively, but before this, a detailed discussion of the reconnection update, which is applied after every move and add update, is in order.

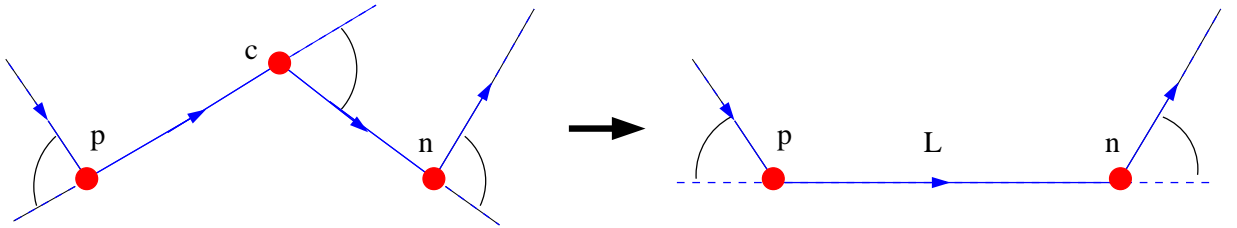


FIG. 4. The delete update deletes the current node (c), joining the connected vortex lines into one between the previous (p) and the next node (n). It affects three and two vortex angles before and after the update, respectively. The new vortex length L has to lie in the range $L_{min} < L < L_{max}$, like for all other updates.

B. Reconnections

If the current node is not deleted, all nodes in a $3 \times 3 \times 3$ volume around the current node are considered for reconnections. The reconnection update causes the cancellation of two close, parallel vortex lines and reconnection of the involved nodes with new vortex lines. Physically, this implements the fact that two vortex lines lying on top of one another is equivalent to no physical flux being present; since the actual vortices being represented are considered to possess a certain thickness, the cancellation can be considered to occur as soon as the vortices significantly overlap, i.e., are sufficiently close and parallel. The terms "close" and "parallel" call for two more parameters in the model, the reconnection length r_r and the reconnection angle ϵ . The shortest distance and the angle between two vortex lines must be smaller than r_r and ϵ respectively, in order to reconnect the four involved nodes with new vortex lines. An illustrative example of the reconnection update is shown in Fig. 5. The lengths of the new vortex lines, as always, have to be smaller than L_{max} ; however, the constraint of minimal distance L_{min} is not enforced in reconnection updates in order to allow for reconnections of almost congruent vortex lines. If all conditions for the reconnection are fulfilled, the update is subjected to the Metropolis algorithm, considering the action of the four nodes involved. The reconnection update allows separation and merging of vortex clusters. It should be noted that the data structure of the vortex nodes imposes an orientation on the vortex clusters (previous, next, etc.). If two merging clusters have opposite orientation, the orientation of one of the clusters is reversed, cf. Fig. 5. This orientation is a technical issue only and has no physical meaning in this model.

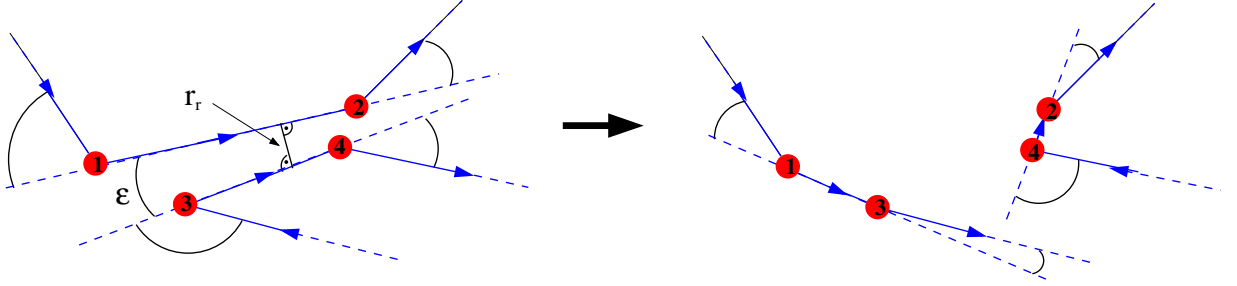


FIG. 5. The reconnection update deletes the vortex lines between nodes 1-2 and 3-4 and reconnects nodes 1-3 and 4-2. The plot shows the affected vortex angles, the reconnection angle ϵ and distance r_r . The plotted vortex lines/nodes might belong to the same or different clusters. Note that the orientation of some vortex lines was reversed in this example, cf. main text.

C. Parameters

This section summarizes all parameters used in the model and the optimized values used for the simulations on $16^2 \times L_T$ volumes. It should be noted that the search for viable parameter sets and update conditions constituted the most demanding part of the simulation effort in this work. This includes tuning for useful acceptance rates for move, add, delete, and reconnection updates as well as new clusters popping up out of the vacuum. In addition, a substantive competition between action and entropy in the ensemble must be maintained to obtain physically interesting behavior.

- Vortex length action parameter $\alpha = 0.11$
In the action $S = \alpha L + \gamma \psi^2$, the vortex segment length L at a node is defined as the distance to the previous node.
- Vortex angle action parameter $\gamma = 0.33$
The vortex angle φ is defined as the angle between the oriented vectors of the vortex lines connecting the previous, current and next nodes, see Fig. 1.
- Maximal vortex segment length $L_{max} = 1.7$
- Minimal vortex segment length $L_{min} = 0.3$
This parameter acts as a minimal length scale in the model, also determining
 - the maximal radius of the move update $r_m = 4L_{min}$, see Fig. 2.
 - the maximal radius of the add update $r_a = 3L_{min}$, see Fig. 3.
 - the reconnection length $r_r = L_{min}$, see Fig. 5.

- Recombination angle $\epsilon = 5^\circ$
 ϵ is the maximal angle between recombining vortex lines, see Fig. 5.
- Vortex density cutoff $d = 8$
 Maximal number of nodes in a $3 \times 3 \times 3$ volume.

D. Monte Carlo Algorithm

For a simulation, the following algorithm was executed a total number of $n_r = n_w + n_m * n_s$ times, where $n_w = 10^4$ is the number of equilibration iterations, $n_m = 2 \dots 5 \times 10^5$ is the number of measurements and $n_s = 10$ the number of sweeps between the measurements.

- The Metropolis algorithm for one 3-node cluster pop-up is called before the node updates; therefore, the new nodes will also be updated before any measurement.
- Monte Carlo sweep over all nodes in the configuration:
 - Metropolis move, add or delete updates are applied to the nodes with rates 66%, 28% and 6%.
 - If a node is not deleted, possible reconnections are considered.
- After the $n_w = 10^4$ equilibration iterations are complete, measurements are performed separated by $n_s = 10$ Monte Carlo sweeps.

The next section introduces the observables measured in the model.

III. OBSERVABLES

The most directly accessible observables in the model are ones associated with the action used to generate the ensemble, e.g., the total action itself and the actual vortex density. These were used to analyze the equilibration phase of the simulations. A number of $n_w = 10^3$ equilibration sweeps was seen to be generally sufficient for the model to thermalize; however, for the following simulations, $n_w = 10^4$ thermalization steps were used. After that, the average action per node, the actual vortex density, the average vortex segment length and angle, and Wilson loops were measured, and a vortex cluster analysis was performed, every $n_s = 10$ Monte Carlo sweeps. Wilson loop and vortex cluster measurements will be detailed below. The vortex density is a nontrivial observable since the cutoff parameter d is applied only for the add update; the vortex node density can locally exceed this cutoff since the vortex nodes can move without density restrictions. The actual vortex density is then given by the node density times the average vortex segment length.

A. Vortex Cluster Analysis

The vortex cluster analysis comprises counting the number of closed vortex clusters, the number of vortex nodes/line segments for each cluster, the cluster size or maximal extent of each cluster and the number of clusters winding around the time dimension. The distribution of vortex flux into clusters of different sizes will be visualized in cluster size histograms binning vortex nodes into 20 bins corresponding to the sizes of the clusters to which they belong, where cluster size is normalized using the maximal possible cluster size s_m . Taking into account the periodic boundary conditions, the maximal possible cluster size is determined by $s_m^2 = L_S^2/2 + L_T^2/4$. In the following analysis, the expression "maximal cluster fraction" will refer to the fraction of vortex nodes/line segments which reside within a cluster of size s_m , *i.e.* the magnitude of the bin of maximal possible cluster size in the aforementioned histograms. This quantifies to what extent vortices percolate. On the other hand, vortex clusters winding around the time dimension are important in particular in the deconfined phase; in the percolation transition separating the confining and the deconfined phase, the large percolating clusters of the confining phase decay into many such winding clusters [12]. The latter are instrumental in maintaining a spatial string tension in the deconfined phase while the physical string tension extracted from temporal Wilson loops vanishes [12]. Monitoring in particular vortices winding around the time dimension therefore provides an additional diagnostic for the deconfining transition. Such vortices can be produced during reconnection updates, either in pairs or even singly if the temporal extent of the torus is sufficiently small ($L_T < 3L_{max}$).

B. Wilson Loops

The Wilson loop $W(R, T)$ along a closed rectangular path in space and time of dimensions $R \times T$ is the observable most frequently used to discuss confinement in lattice gauge theory. It can be interpreted in terms of the creation of a static quark–anti-quark pair with a certain spatial separation R , its evolution for a time T , and its subsequent annihilation. The effective action associated with this process yields the potential energy contained in the static quark–anti-quark pair. Center vortices have a characteristic effect on Wilson loops; each center vortex linked with a Wilson loop (or, equivalently, piercing any area spanned by the loop) contributes a multiplicative factor to the loop corresponding to a center element of the gauge group. This can, indeed, be viewed as the defining property of a center vortex; it specifies the flux carried by the vortex, which is measured by a Wilson loop encircling it. In the case of the $SU(2)$ gauge group considered here, the only non-trivial center element is -1 ; this is the factor by which any Wilson loop linked to a vortex is multiplied.

To evaluate Wilson loops in the present model, it is sufficient to examine all vortex line segments in a configuration, determining whether each line segment pierces the planar area spanned by the Wilson loop in question, and supplying a factor -1 to the Wilson loop for each piercing (if there are no piercings, $W(R, T) = 1$). Using the fact that larger Wilson loops are simply given by products of smaller Wilson loops with which the larger loop can be tiled, one can organize the calculation of a large number of Wilson loops on a given configuration efficiently. The expectation value of the time-like Wilson loops $\langle W(R, T) \rangle$ yields the quark–anti-quark potential,

$$V(R) = - \lim_{T \rightarrow \infty} \ln \langle W(R, T) \rangle / T . \quad (2)$$

To extract the string tension σ of the system, an ansatz $V(R) = \sigma R + C/R + V_0$ is fitted to the potentials. The spatial string tension σ_s is obtained from spatial Wilson loops using Creutz ratios,

$$\chi(R) = - \ln \left(\frac{\langle W(R, R) \rangle \langle W(R+1, R+1) \rangle}{\langle W(R+1, R) \rangle \langle W(R, R+1) \rangle} \right) \xrightarrow{R \rightarrow \infty} \sigma_s . \quad (3)$$

The spatial string tension is expected to be correlated with the number of vortex clusters winding in time direction, since these vortices will pierce the spatial Wilson loops.

IV. RESULTS & DISCUSSION

A. Finite temperature phase transition from varying temporal extent L_T

In this section, we study center vortex ensembles at different temperatures. The following results were obtained on volumes $16^2 \times L_T$ for a range of inverse temperatures L_T in order to resolve the deconfining phase transition at different vortex density cutoffs $d = 4, 6, 8, 10$ and 12 , with $L_{max} = 1.7$ and $L_{min} = 0.3$. In Fig. 6 we show the results extracted for $d = 4$, namely, the cluster size histogram, the potential $V(R)$ between the quark and anti-quark and the spatial and temporal string tensions as well as the maximal cluster fraction as a function of temperature. For all other densities ($d = 6 \dots 12$) we show the cluster size histograms in Fig. 10 and string tensions resp. maximal cluster fractions vs. temperature in Fig. 7. In the $d = 4$ case (Fig. 6) we observe a phase transition in the vicinity of the inverse temperatures $L_T = 5, 6$. The cluster size histogram in Fig. 6a shows no cluster percolating through the physical volume for $L_T = 4$, whereas from $L_T = 7$ onwards one large percolating cluster starts to dominate the configuration. The quark–anti-quark potential shown in Fig. 6b is still flat (asymptotically) for $L_T = 5$, while a linearly rising behavior is evident by $L_T = 9$. In between, the potentials do not show a clear linear behavior, and the determination of the string tension is somewhat ambiguous; however, a deviation of the potential below an exactly linear behavior is to be expected in view of the finite spatial extent of the physical volume and the periodic boundary conditions. In the $d = 4$ case, thus, the deconfining transition is not very sharply defined; this is associated with the rather small density cutoff d , as is revealed by examination of higher values of d .

For higher vortex densities, the phase transition becomes much sharper and the inverse critical temperature tends to smaller temporal extents L_T . This can be seen in Fig. 7 and especially Fig. 8, which summarizes the results on the finite temperature phase transition for various vortex density cutoffs d , and also in the corresponding cluster size histograms in Fig. 10 where one should note the different coloring and temperatures for the individual plots. We locate the phase transition for $d = 6$ in the vicinity of $L_T = 2$, for $d = 8$ in the vicinity of $L_T = 1.6$, for $d = 10$ in the vicinity of $L_T = 1.5$ and for $d = 12$ in the vicinity of $L_T = 1.2$. Further, we notice that Fig. 6c and the plots in Fig. 7 show a perfect agreement between the confinement (string tension) and percolation (maximal cluster fraction) transitions. In Fig. 11 we show sample configurations for various temperatures and density cutoff $d = 4$. While for

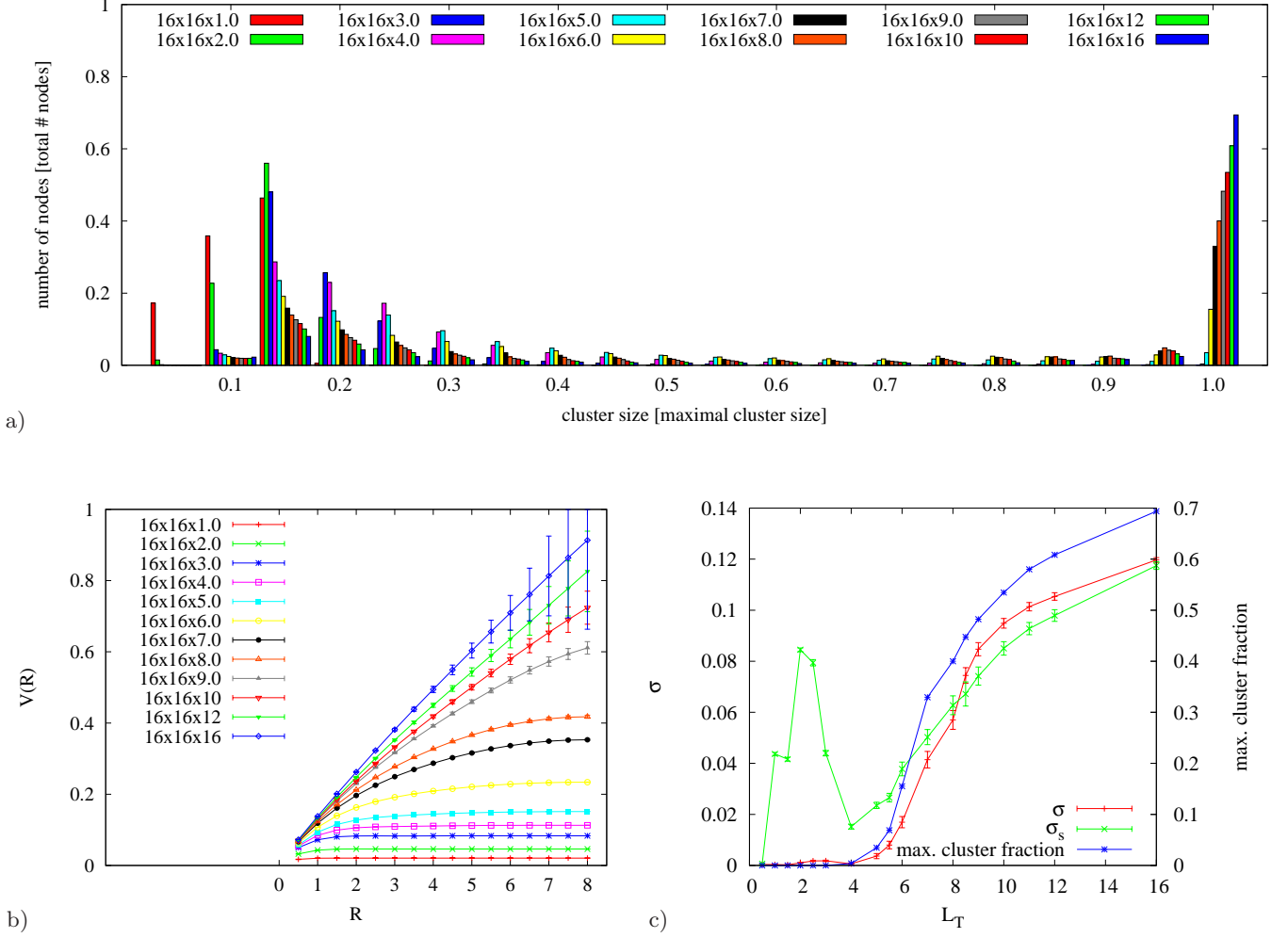


FIG. 6. a) Cluster size histogram, b) quark-anti-quark potentials and c) maximal cluster fraction, temporal and spatial string tensions σ and σ_s for $16^2 \times L_T$ volumes, density cutoff $d = 4$, vortex lengths $L_{max} = 1.7$, $L_{min} = 0.3$.

$L_T = 2$ and 4 (Fig. 11a and b) we see many small vortex clusters, we observe already one big cluster extending over the whole physical volume together with some small clusters for $L_T = 8$ (Fig. 11c) while for $L_T = 16$ (zero temperature, Fig. 11d) it appears as though almost all nodes were connected. In fact, the careful observer can still make out a few three- and four-node clusters, *e.g.*, at the bottom left corner of the 3D plot in Fig. 11d, and indeed we still have around 25-30 individual clusters in this configuration, see Fig. 9 for the average number of clusters within a configuration at different inverse temperatures L_T and vortex densities d . Nevertheless, the majority ($\approx 70\%$, see Fig. 6a and c) of nodes in Fig. 11d is part of one big cluster percolating through the whole physical volume, indicating a confined phase.

It remains to discuss the spatial string tension, which at first sight seems to display unusual behavior in Figs. 6c and 7. Apart from the fact that the behavior at very small L_T becomes unphysical, because the lower bound on the vortex segment length L_{min} artificially suppresses vortices winding around the time direction, one would expect that the spatial string tension remains more or less constant across the deconfining transition; after all, spatial Wilson loops will still be pierced by vortex clusters winding in the time direction even once the percolation effect ceases. However, it appears that these two effects to a certain extent disentangle and are separated as a function of L_T . For $d = 4$ we clearly see a decreasing spatial string tension with increasing temperature, in accordance with loss of percolation in the vicinity of the percolation transition, while only below $L_T = 4$, (*i.e.*, above the transition temperature) the effect of winding vortices sets in. Note that (much weaker) hints of such behavior are also seen in vortex ensembles extracted from lattice Yang-Mills configurations [10]. In Fig. 9b we plot the number of vortices winding around the time direction; the correlation of these windings with the behavior seen in the spatial string tension for $d = 4$ is clearly visible. For higher densities, percolation and winding effects become more entangled and harder to distinguish.

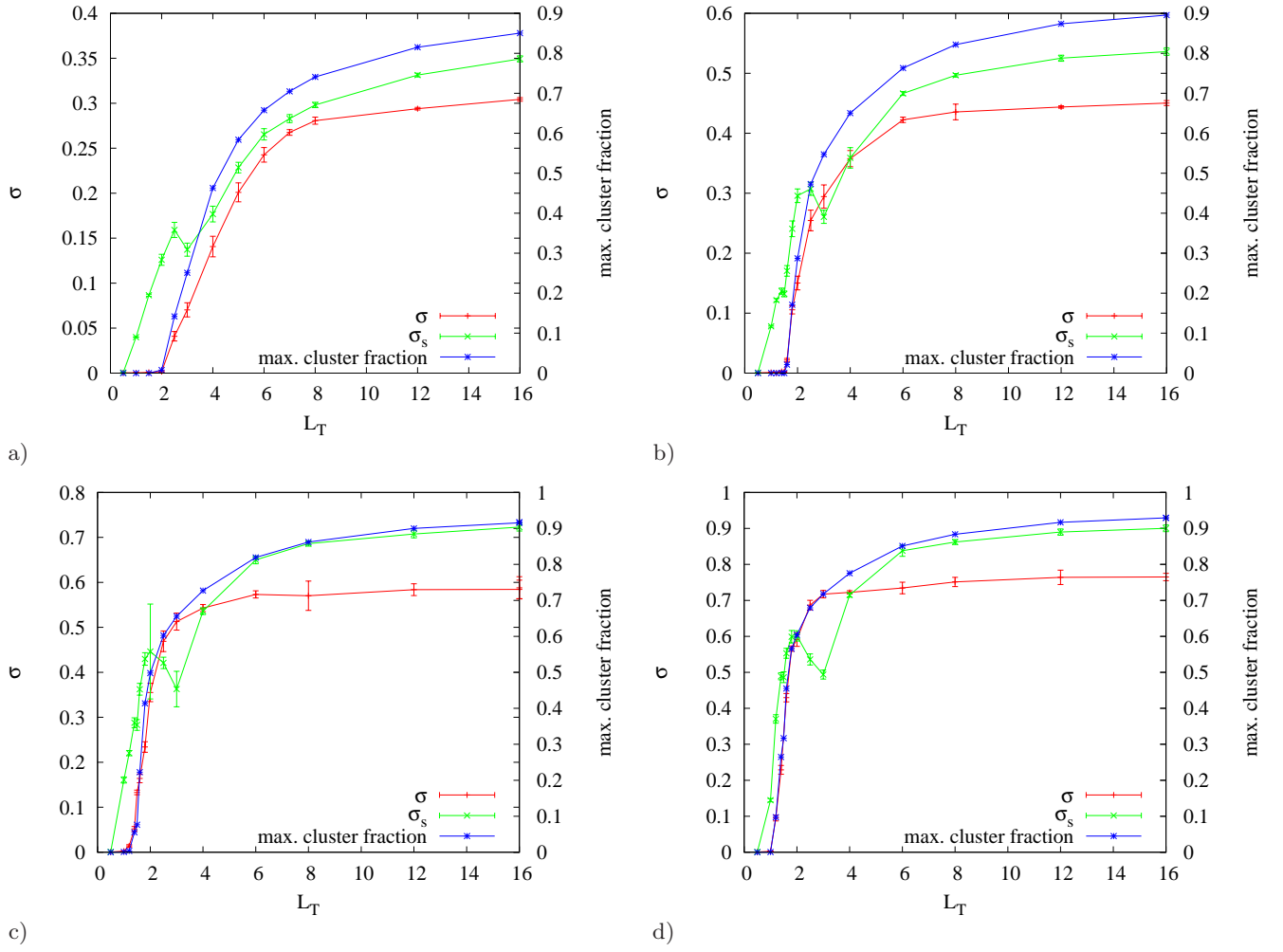


FIG. 7. Maximal cluster fraction, temporal and spatial string tensions σ and σ_s for $16^2 \times L_T$ volumes, density cutoff a) $d = 6$, b) $d = 8$, c) $d = 10$, d) $d = 12$, vortex lengths $L_{max} = 1.7$, $L_{min} = 0.3$.

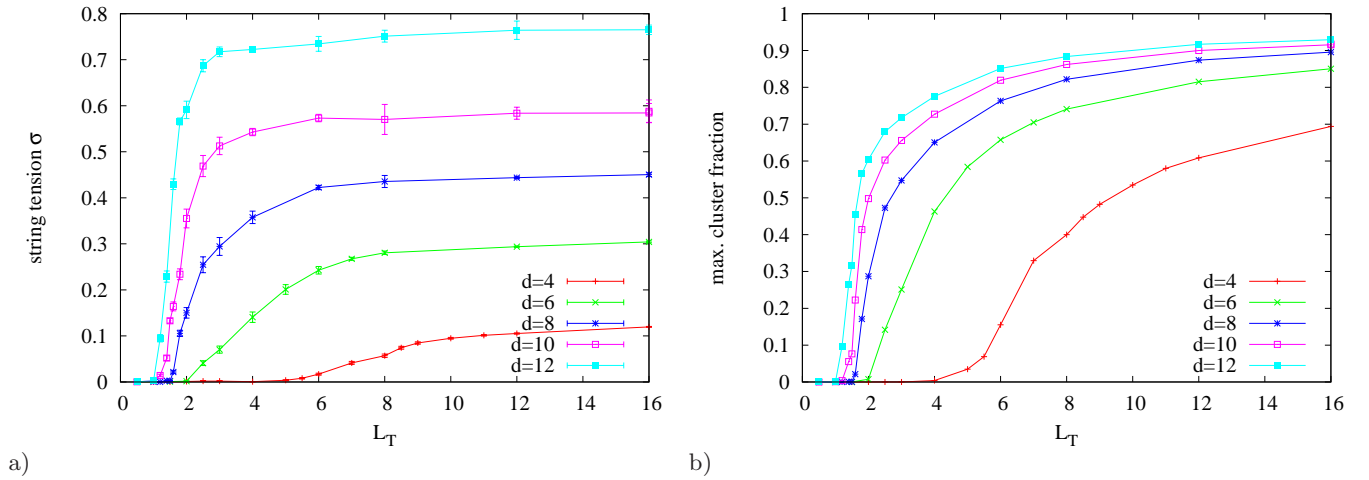


FIG. 8. String tension σ and maximal cluster fraction vs. time extent L_T of $16^2 \times L_T$ volumes, for different density cutoffs, vortex lengths $L_{max} = 1.7$, $L_{min} = 0.3$.

Examining once more Fig. 9, we observe that the total number of vortex clusters peaks around the deconfinement temperature in all cases. This peak is rather weak for $d = 4$, but becomes stronger as d is allowed to rise. The behavior of the plots in Fig. 9 converges with rising d ; only the $d = 4$ case is fairly strongly separated from the ones at higher d . By $d = 8$, the behavior of the vortex configurations appears to have converged, and the finite temperature transition seen in Fig. 8 has become sharp. For this reason, we choose $d = 8$ for the analysis of the dependence on vortex segment length range in Secs. IV C and IV D.

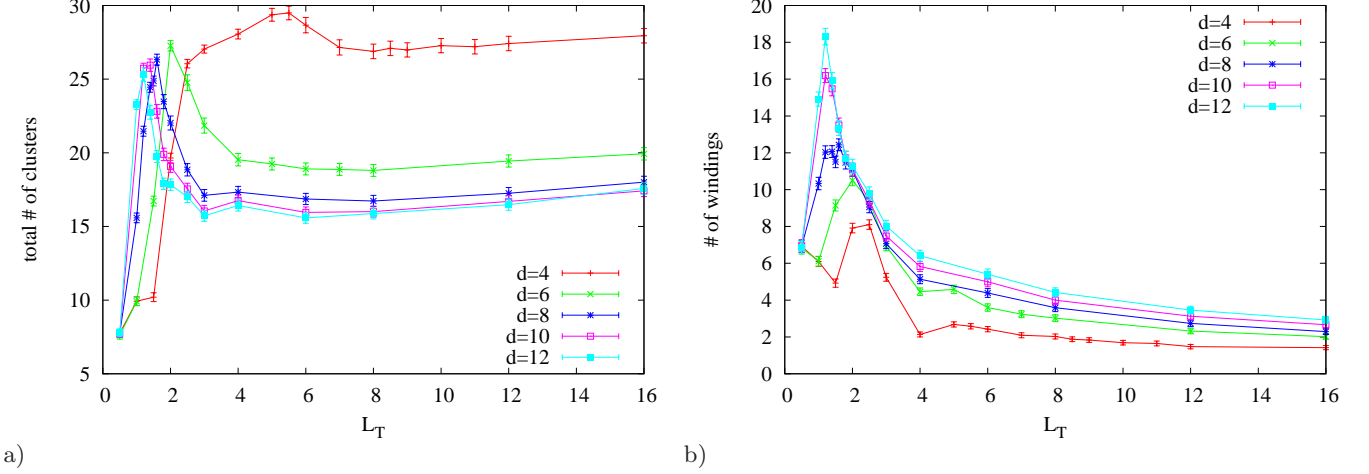


FIG. 9. a) Total number of vortex clusters and b) windings around the temporal dimension, on $16 \times L_T$ volumes, for vortex lengths $L_{max} = 1.7$, $L_{min} = 0.3$.

B. Deconfining transition as a function of vortex density cutoff d

In this section, we investigate the random vortex line ensembles for varying density cutoff $d = 4 \dots 13$ on three different physical volumes $16^2 \times L_T$ with $L_T = 2 \dots 4$, $L_{max} = 1.7$ and $L_{min} = 0.3$. In Fig. 12 we show the quark–anti-quark potentials on a $16^2 \times 2$ volume, as well as the string tensions σ and σ_s and the maximal vortex cluster fraction as a function of d for the various L_T . In Fig. 13 we show the corresponding cluster size histograms. We observe a deconfinement transition with respect to the vortex density cutoff d . At $d = 4$ all cases are in the deconfined phase; the $L_T = 4$ configurations then immediately start to confine when d is increased, whereas the $L_T = 3$ and $L_T = 2$ configurations reach the transition around $d = 5$ and $d = 6$, respectively. Again, the confinement and percolation transitions (Fig. 12b and d) agree perfectly; the maximal clusters in Fig. 13 start to develop at exactly the aforementioned critical densities. Higher densities of course allow for more reconnections and percolation, *i.e.*, they facilitate confinement. The spatial string tension at $d = 4$ essentially vanishes in the $L_T = 4$ case with percolation having ceased and almost no winding vortex clusters present to counteract the decline; on the other hand, for $L_T = 3$ and $L_T = 2$, the effect of winding vortices already manifests itself at $d = 4$ in a stabilization of the spatial string tension at finite values. This interplay was discussed in more detail already in the previous section.

C. Phase transition from varying maximal vortex length L_{max}

In this section, we investigate the behavior of the ensembles at different maximal vortex segment lengths $L_{max} = 1.0 \dots 2.2$ for a physical volume $16^2 \times 2$ and a density cutoff $d = 8$, with $L_{min} = 0.3$. In Fig. 14 we show the cluster size histogram, the quark–anti-quark potential, and string tensions σ and σ_s as well as maximal cluster fraction versus the different maximal vortex segment lengths L_{max} .

In this case, we observe a well-defined phase transition at $L_{max} = 1.5$, with no percolation and string tension σ , *i.e.*, a flat quark–anti-quark potential below that threshold, and percolation resp. confinement above. Restricting the vortex line segment length to a more stringent upper bound shifts the action-entropy balance away from the entropy-dominated regime and leads to small, separated vortex clusters which cannot reconnect or percolate, and confinement is lost. Evidently, also the spatial string tension in the deconfined phase decreases as the L_{max} bound becomes more stringent, indicating that the number of vortices winding in the time direction is likewise suppressed.

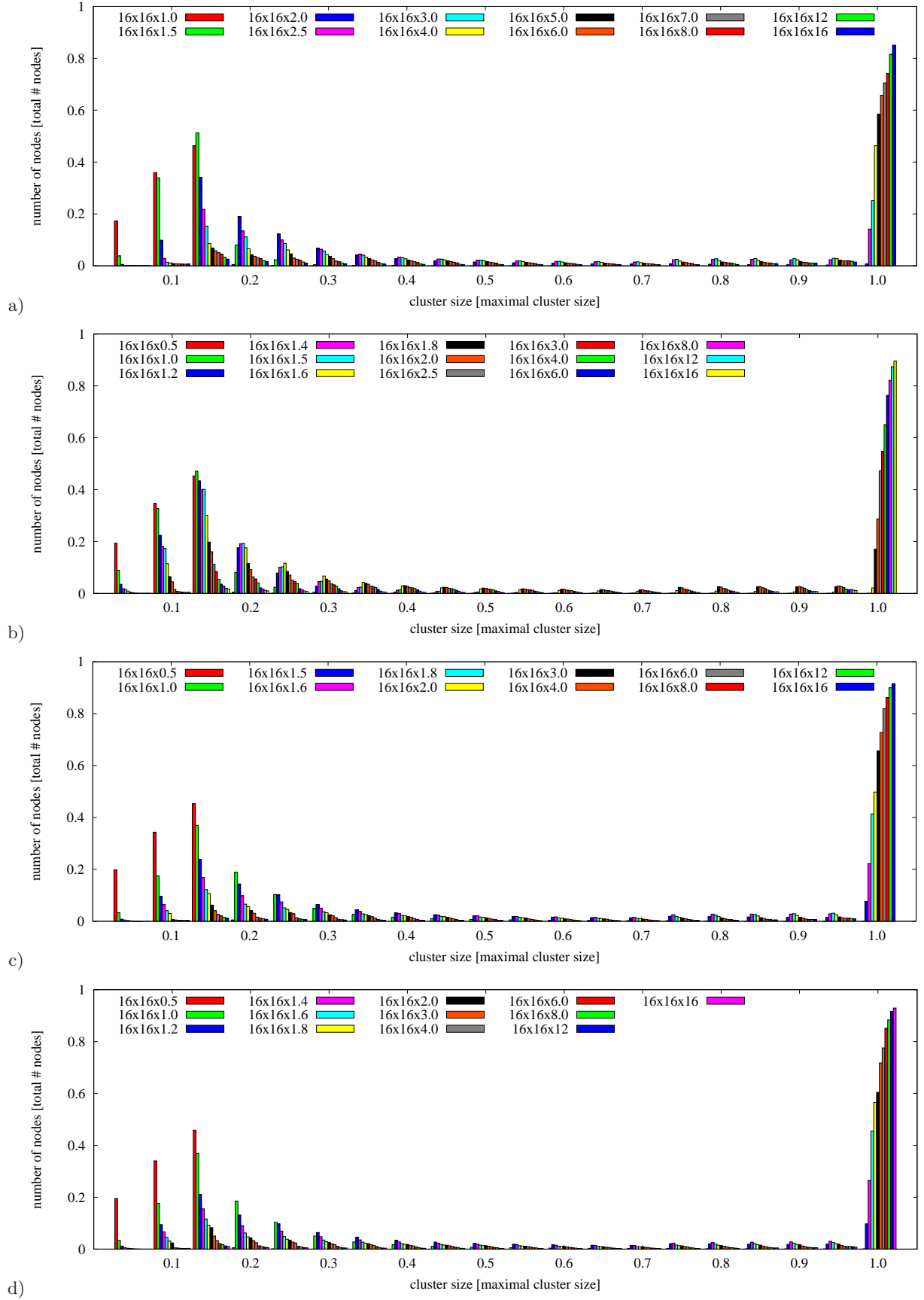


FIG. 10. Cluster size histograms for $16^2 \times L_T$ volumes, density cutoff a) $d = 6$, b) $d = 8$, c) $d = 10$, d) $d = 12$, vortex lengths $L_{max} = 1.7$, $L_{min} = 0.3$.

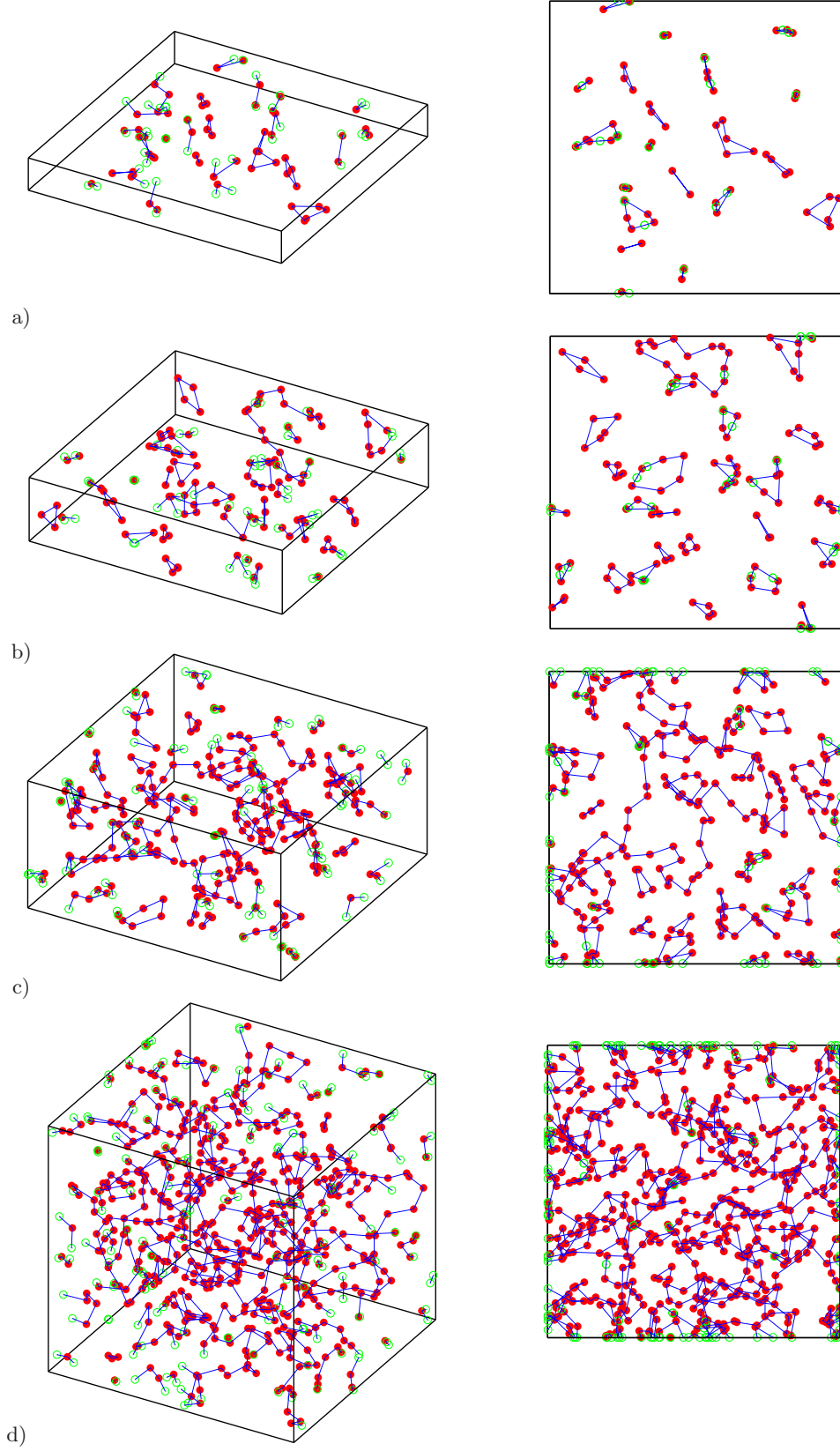


FIG. 11. $16^2 \times$ a) 2, b) 4, c) 8 and d) 16 sample configurations, density cutoff $d = 4$, vortex lengths $L_{max} = 1.7, L_{min} = 0.3$. The right-hand views are directly into the temporal direction.

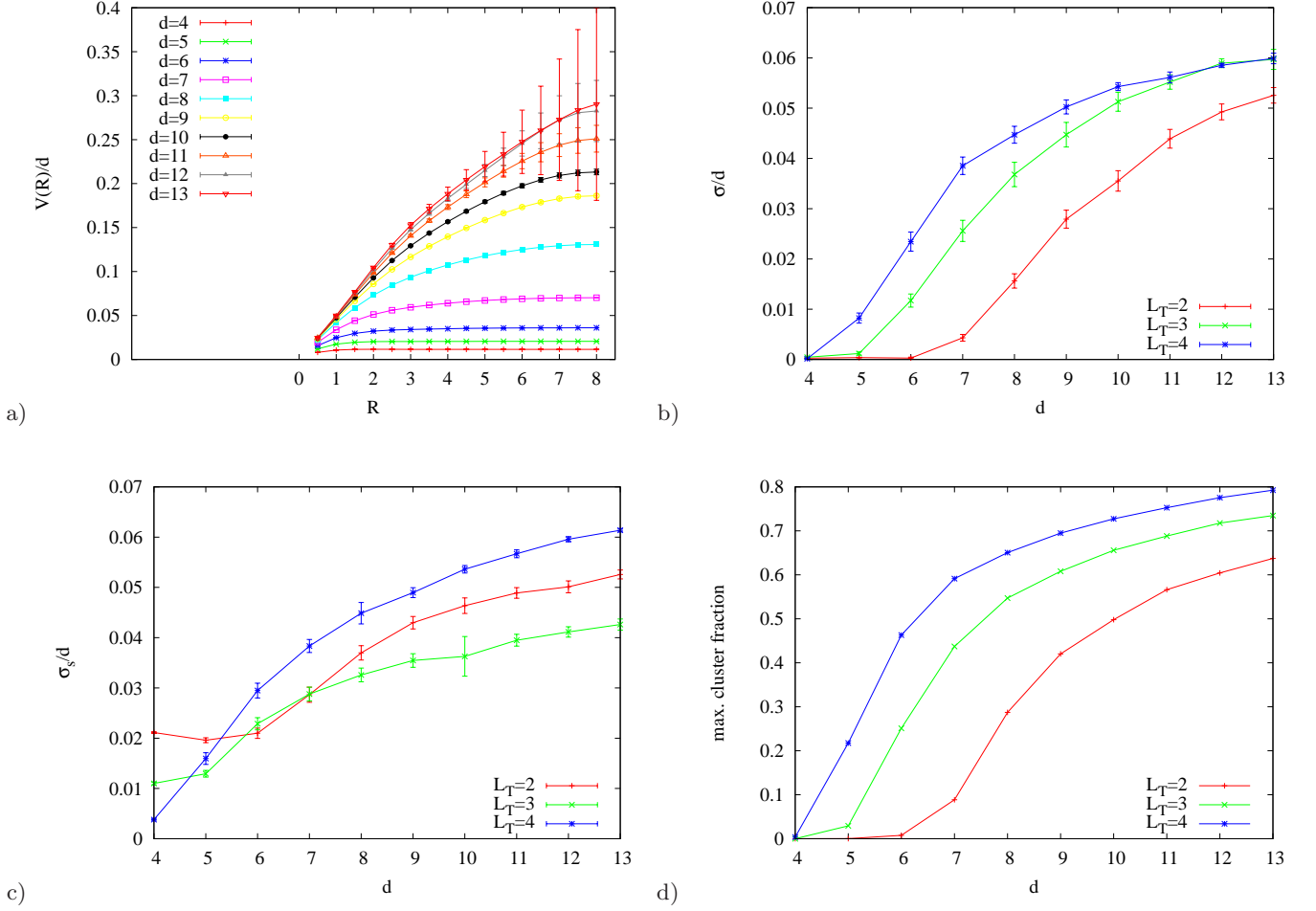


FIG. 12. a) Quark-anti-quark potentials on a $16^2 \times 2$ volume, string tensions b) σ , c) σ_s and d) maximal vortex cluster fraction as a function of density cutoff d for $16^2 \times L_T$ volumes and vortex lengths $L_{max} = 1.7$, $L_{min} = 0.3$.

D. Behavior as a function of minimal vortex/reconnection length L_{min}

The interpretation of the phase space with respect to the minimal vortex segment length L_{min} is more complex than with respect to other parameters. L_{min} defines a minimal length scale which enters a number of effects governing the vortices; it not only restricts the minimal length of a vortex segment itself, but also determines the maximal move radius $r_m = 4L_{min}$, the maximal add radius $r_a = 3L_{min}$ and the reconnection distance $r_r = L_{min}$. That means that if we choose a small L_{min} , the vortex clusters will not spread out very quickly and reconnections are strongly suppressed. On the other hand, a large L_{min} restricts the set of available configurations, and thus drives the system away from the entropy-dominated regime, while at the same time obstructing equilibration, with large attempted updates and frequent recombinations. Both limits do not realize the physical behavior we want to study, and our analysis of configurations in $16^2 \times 2$ volumes with vortex density $d = 8$, maximal vortex length $L_{max} = 1.7$ and varying L_{min} seems to confirm these expectations. The aforementioned set of fixed parameters lies close to the critical point for all the deconfining phase transitions studied further above, *i.e.*, as a function of temperature, vortex density and maximal vortex segment length L_{max} . In Fig. 15 we plot the cluster size histogram, the quark-anti-quark potentials, string tensions σ , σ_s and maximal cluster fraction as well as average vortex node action and vortex density versus $L_{min} = 0.1 \dots 0.7$ in steps of 0.05. We observe deconfined phases for both very small and very large L_{min} . In the former case, the configurations remain rather static and do not readily recombine and percolate; in the latter case, the space of configurations is restricted, leading to a suppressed vortex density which also does not exhibit good percolation properties. At $L_{min} = 0.3$, however, we find a common maximum for string tensions, maximal cluster fraction and average vortex density, and simultaneously the average action shows a minimum. This validates our initial choice for $L_{min} = 0.3$, which appears to yield rather stable ensembles that permitted reliable studies of the phase transitions investigated further above.

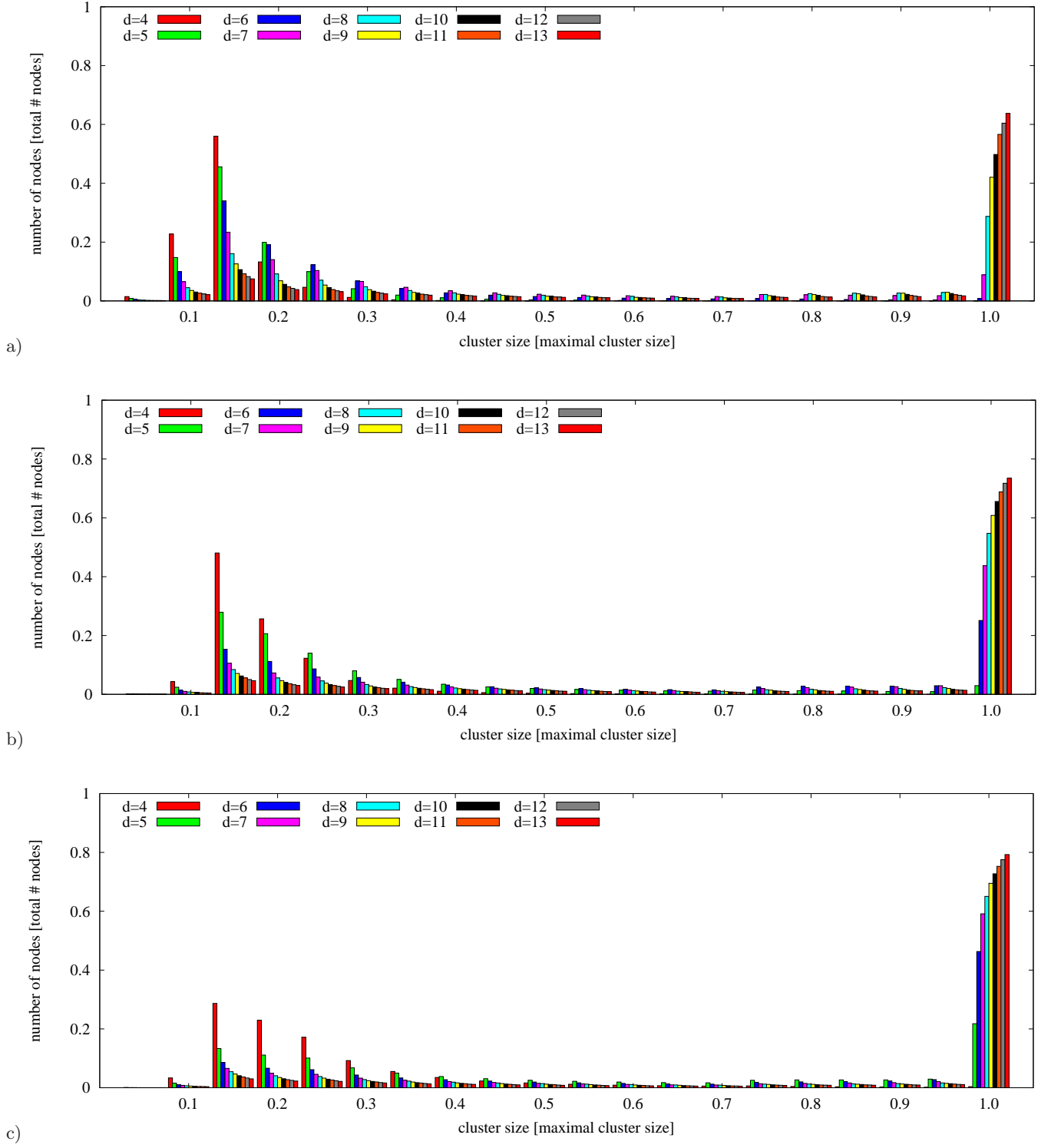


FIG. 13. Cluster size histograms for a) 16×2 b) 16×3 c) 16×4 volumes and different density cutoffs d , vortex lengths $L_{max} = 1.7$, $L_{min} = 0.3$.

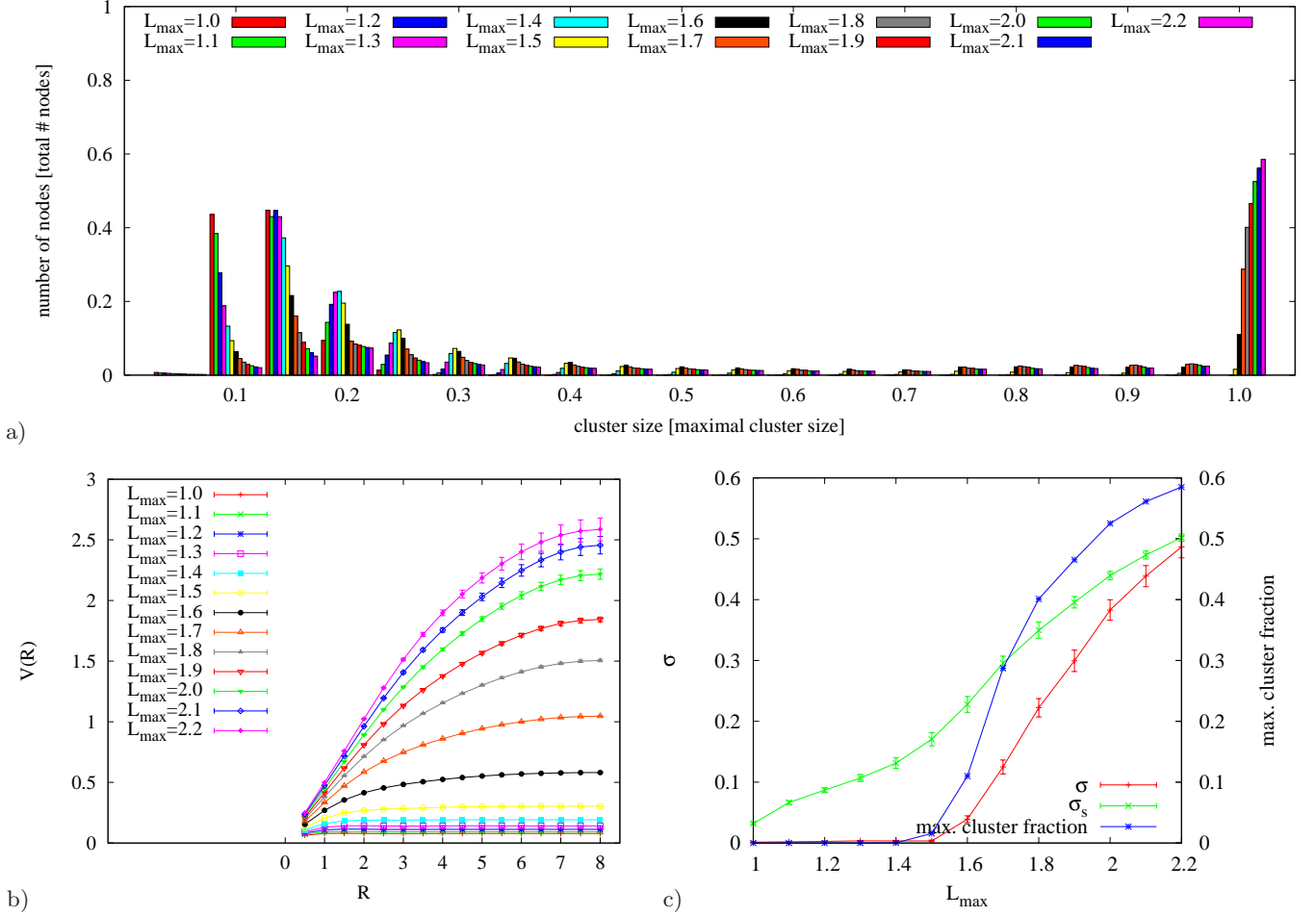


FIG. 14. a) Cluster size histogram, b) quark-anti-quark potential and c) string tensions σ and σ_s as well as maximal cluster fraction as a function of maximal vortex segment length L_{\max} , for a 16×2 volume, density cutoff $d = 8$ and $L_{\min} = 0.3$.

V. CONCLUSIONS & OUTLOOK

We presented a $2 + 1$ -dimensional center vortex model of the Yang-Mills vacuum. The vortices are represented by closed random lines which are modeled as being piece-wise linear, and an ensemble is generated by Monte Carlo methods. The physical space in which the vortex lines are defined is a torus with periodic boundary conditions. The motivation for this study was to explore a formulation which avoids the shortcomings of previous realizations of random center vortex models that relied on a hypercubic scaffolding for the construction of the vortex configurations. The present formulation preserves translational and rotational symmetry, and updates can occur continuously in space-time. Vortex configurations are allowed to grow and shrink, and also reconnections are allowed, *i.e.*, vortex lines may fuse or disconnect. Our ensemble therefore contains not a fixed, but a variable number of closed vortex lines. This is in fact a crucial ingredient for achieving a system of percolating vortices, *i.e.*, a confining phase. All vortex updates (move, add, delete, reconnect) are subjected to a Metropolis algorithm driven by an action depending on vortex segment length and the angle between two adjacent vortex segments; *i.e.*, the action contains both a length and a curvature term. After tuning all necessary parameters, which are summarized in section II C, we use the model to study both vortex percolation and the potential $V(R)$ between quark and anti-quark as a function of distance R at different vortex densities, vortex segment length ranges, reconnection conditions and at different temperatures (by varying the temporal extent of the physical volume).

We have found three deconfinement transitions, namely, as a function of density, as a function of vortex segment length range, and as a function of temperature. The deconfinement transitions coincide with percolation transitions in the vortex configurations. For small vortex densities and restricted vortex segment lengths, the configurations consist of small, independent vortex clusters, and for high temperatures, vortex clusters prefer to separate and wind around the (short) temporal extent of the volume; in these cases, there is no percolation, the quark-anti-quark potentials

show no linearly rising behavior, *i.e.*, no string tension is measured, and the system is in the deconfined phase. Once one allows for higher vortex densities, less restricted vortex segment lengths, or larger temporal extent, *i.e.*, lower temperature, the vortex configurations begin to percolate; small clusters reconnect to mainly one large vortex cluster filling the whole volume. In this regime, we measure a finite string tension, *i.e.* linearly rising quark–anti-quark potentials; hence the vortices confine quarks and anti-quarks.

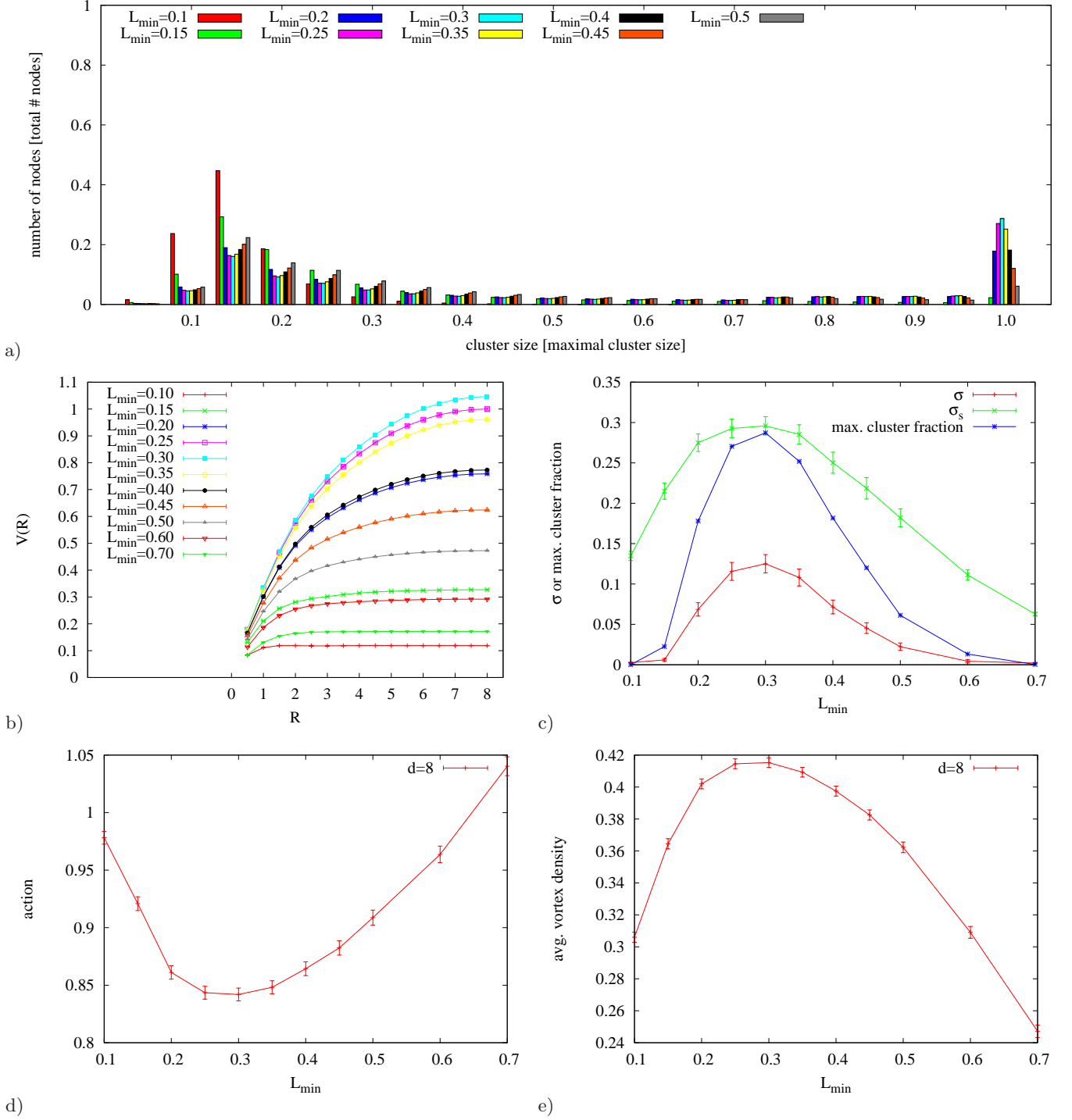


FIG. 15. a) Cluster size histogram, b) quark–anti-quark potential, c) string tensions and maximal vortex cluster fraction, average d) node action and e) vortex line density (= avg. node density \times avg. vortex length) for 16×2 volumes, density cutoff $d = 8$ and different vortex/reconnection lengths L_{\min} at $L_{\max} = 1.7$.

The physically most relevant extension of the modeling effort presented here is of course the one to $D = 4$ space-time dimensions, where center vortices are described by 2-dimensional random world-surfaces. The surfaces can be represented by random triangulations, anchored again by nodes which can move, be added, or deleted from configurations. Surface separation at bottlenecks, and the converse process of fusing of surfaces constitute crucial ingredients for achieving percolating configurations. In these $D = 4$ ensembles, one can then model Yang-Mills topological properties in addition to the confinement properties. A sobering lesson of the present exploratory study is the proliferation of modeling parameters in the type of formulation investigated here, compared to previous models utilizing a hypercubic scaffolding. This of course restricts the predictive potential of such models. Nevertheless, it has proven possible to reproduce the qualitative features of confinement physics seen in $SU(2)$ Yang-Mills theory within the formulation constructed here.

ACKNOWLEDGMENTS

We thank S. Catterall and D. A. Johnston for helpful discussions. This research was supported by the U.S. DOE through grant DE-FG02-96ER40965 (D.A.,M.E.) and the Erwin Schrödinger Fellowship program of the Austrian Science Fund FWF (“Fonds zur Förderung der wissenschaftlichen Forschung”) under Contract No. J3425-N27 (R.H.).

-
- [1] G. 't Hooft, “On the phase transition towards permanent quark confinement,” *Nucl. Phys.* **B138** (1978) 1.
 - [2] P. Vinciarelli, “Fluxon solutions in nonabelian gauge models,” *Phys. Lett.* **B78** (1978) 485–488.
 - [3] T. Yoneya, “ $Z(n)$ topological excitations in yang-mills theories: Duality and confinement,” *Nucl. Phys.* **B144** (1978) 195.
 - [4] J. M. Cornwall, “Quark confinement and Vortices in massive gauge invariant QCD,” *Nucl. Phys.* **B157** (1979) 392.
 - [5] G. Mack and V. B. Petkova, “Comparison of Lattice Gauge Theories with gauge groups $Z(2)$ and $SU(2)$,” *Ann. Phys.* **123** (1979) 442.
 - [6] H. B. Nielsen and P. Olesen, “A Quantum Liquid Model for the QCD Vacuum: Gauge and Rotational Invariance of Domained and Quantized Homogeneous Color Fields,” *Nucl. Phys.* **B160** (1979) 380.
 - [7] L. Del Debbio, M. Faber, J. Greensite, and Š. Olejník, “Center dominance and $Z(2)$ vortices in $SU(2)$ lattice gauge theory,” *Phys. Rev. D* **55** (1997) 2298–2306, [arXiv:9610005 \[hep-lat\]](#).
 - [8] K. Langfeld, H. Reinhardt, and O. Tennert, “Confinement and scaling of the vortex vacuum of $SU(2)$ lattice gauge theory,” *Phys. Lett.* **B419** (1998) 317–321, [arXiv:9710068 \[hep-lat\]](#).
 - [9] L. Del Debbio, and M. Faber, and J. Greensite, and Š. Olejník, “Center dominance, center vortices, and confinement,” [arXiv:9708023 \[hep-lat\]](#).
 - [10] K. Langfeld, O. Tennert, M. Engelhardt, and H. Reinhardt, “Center vortices of Yang-Mills theory at finite temperatures,” *Phys. Lett.* **B452** (1999) 301, [arXiv:9805002 \[hep-lat\]](#).
 - [11] T. G. Kovacs and E. T. Tomboulis, “Vortices and confinement at weak coupling,” *Phys. Rev. D* **57** (1998) 4054–4062, [arXiv:9711009 \[hep-lat\]](#).
 - [12] M. Engelhardt and H. Reinhardt, “Center vortex model for the infrared sector of Yang-Mills theory: Confinement and deconfinement,” *Nucl. Phys.* **B585** (2000) 591–613, [arXiv:hep-lat/9912003 \[hep-lat\]](#).
 - [13] M. Engelhardt, K. Langfeld, H. Reinhardt, and O. Tennert, “Deconfinement in $SU(2)$ Yang-Mills theory as a center vortex percolation transition,” *Phys. Rev. D* **61** (2000) 054504, [arXiv:hep-lat/9904004 \[hep-lat\]](#).
 - [14] R. Bertle and M. Faber, “Vortices, confinement and Higgs fields,” [arXiv:0212027 \[hep-lat\]](#).
 - [15] M. Engelhardt, M. Quandt, and H. Reinhardt, “Center vortex model for the infrared sector of $SU(3)$ Yang-Mills theory: Confinement and deconfinement,” *Nucl. Phys.* **B685** (2004) 227–248, [arXiv:0311029 \[hep-lat\]](#).
 - [16] R. Höllwieser, D. Altarawneh, and M. Engelhardt, “Random center vortex lines in continuous 3D space-time,” *AIP Conf. Proc.* **1701**, **ConfinementXI** (2014) 030007. <http://scitation.aip.org/content/aip/proceeding/aipcp/10.1063/1.4938613>.
 - [17] D. Altarawneh, R. Höllwieser and M. Engelhardt, “Confining Bond Rearrangement in Random Center Vortex Models,” (*accepted by PRD*) (2015), [arXiv:1508.07596 \[hep-lat\]](#).
 - [18] R. Höllwieser and D. Altarawneh, “Center Vortices, Area Law and the Catenary Solution,” *Int. J. Mod. Phys. A* **30** (2015) 1550207, [arXiv:1509.00145 \[hep-lat\]](#).
 - [19] J. Greensite, “The confinement problem in lattice gauge theory,” *Prog. Part. Nucl. Phys.* **51** (2003) 1, [arXiv:hep-lat/0301023 \[hep-lat\]](#).
 - [20] J. Greensite and R. Höllwieser, “Double-winding Wilson loops and monopole confinement mechanisms,” *Phys. Rev. D* **91** no. 5, (2015) 054509, [arXiv:1411.5091 \[hep-lat\]](#).
 - [21] R. Bertle, M. Engelhardt, and M. Faber, “Topological susceptibility of Yang-Mills center projection vortices,” *Phys. Rev. D* **64** (2001) 074504, [arXiv:0104004 \[hep-lat\]](#).
 - [22] M. Engelhardt, “Center vortex model for the infrared sector of Yang-Mills theory: Topological susceptibility,” *Nucl. Phys.* **B585** (2000) 614, [arXiv:0004013 \[hep-lat\]](#).

- [23] M. Engelhardt, “Center vortex model for the infrared sector of SU(3) Yang-Mills theory: Topological susceptibility,” *Phys. Rev. D* **83** (2011) 025015, [arXiv:1008.4953 \[hep-lat\]](#).
- [24] R. Höllwieser, M. Faber, U.M. Heller, “Lattice Index Theorem and Fractional Topological Charge,” [arXiv:1005.1015 \[hep-lat\]](#).
- [25] R. Höllwieser, M. Faber, U.M. Heller, “Intersections of thick Center Vortices, Dirac Eigenmodes and Fractional Topological Charge in SU(2) Lattice Gauge Theory,” *JHEP* **1106** (2011) 052, [arXiv:1103.2669 \[hep-lat\]](#).
- [26] T. Schweigler, R. Höllwieser, M. Faber and U.M. Heller, “Colorful SU(2) center vortices in the continuum and on the lattice,” *Phys.Rev.* **D87** no. 5, (2013) 054504, [arXiv:1212.3737 \[hep-lat\]](#).
- [27] R. Höllwieser, M. Faber, U.M. Heller, “Critical analysis of topological charge determination in the background of center vortices in SU(2) lattice gauge theory,” *Phys. Rev. D* **86** (2012) 014513, [arXiv:1202.0929 \[hep-lat\]](#).
- [28] R. Höllwieser and M. Engelhardt, “Smearing Center Vortices,” *PoS LAT2014* (2014) 356, [arXiv:1411.7097 \[hep-lat\]](#).
- [29] R. Höllwieser and M. Engelhardt, “Approaching SU(2) gauge dynamics with smeared Z(2) vortices,” *Phys. Rev. D* **92** (2015) 034502, [arXiv:1503.00016 \[hep-lat\]](#).
- [30] P. de Forcrand and M. D’Elia, “On the relevance of center vortices to QCD,” *Phys. Rev. Lett.* **82** (1999) 4582–4585, [arXiv:hep-lat/9901020 \[hep-lat\]](#).
- [31] C. Alexandrou, P. de Forcrand, and M. D’Elia, “The role of center vortices in QCD,” *Nucl. Phys.* **A663** (2000) 1031–1034, [arXiv:hep-lat/9909005 \[hep-lat\]](#).
- [32] M. Engelhardt and H. Reinhardt, “Center projection vortices in continuum Yang-Mills theory,” *Nucl. Phys.* **B567** (2000) 249, [arXiv:9907139 \[hep-th\]](#).
- [33] H. Reinhardt and M. Engelhardt, “Center vortices in continuum yang-mills theory,” in *Quark Confinement and the Hadron Spectrum IV*, W. Lucha and K. M. Maung, eds., pp. 150–162. World Scientific, 2002. [arXiv:0010031 \[hep-th\]](#).
- [34] M. Engelhardt, “Center vortex model for the infrared sector of Yang-Mills theory: Quenched Dirac spectrum and chiral condensate,” *Nucl.Phys.* **B638** (2002) 81–110, [arXiv:hep-lat/0204002 \[hep-lat\]](#).
- [35] D. Leinweber, P. Bowman, U. Heller, D. Kusterer, K. Langfeld, *et al.*, “Role of centre vortices in dynamical mass generation,” *Nucl.Phys.Proc.Suppl.* **161** (2006) 130–135.
- [36] V. Bornyakov *et al.*, “Interrelation between monopoles, vortices, topological charge and chiral symmetry breaking: Analysis using overlap fermions for SU(2),” *Phys. Rev. D* **77** (2008) 074507, [arXiv:0708.3335 \[hep-lat\]](#).
- [37] R. Höllwieser, M. Faber, J. Greensite, U.M. Heller, and Š. Olejník, “Center Vortices and the Dirac Spectrum,” *Phys. Rev. D* **78** (2008) 054508, [arXiv:0805.1846 \[hep-lat\]](#).
- [38] P. O. Bowman, K. Langfeld, D. B. Leinweber, A. Sternbeck, L. von Smekal, *et al.*, “Role of center vortices in chiral symmetry breaking in SU(3) gauge theory,” *Phys.Rev.* **D84** (2011) 034501, [arXiv:1010.4624 \[hep-lat\]](#).
- [39] R. Höllwieser, T. Schweigler, M. Faber and U.M. Heller, “Center Vortices and Chiral Symmetry Breaking in SU(2) Lattice Gauge Theory,” *Phys.Rev.* **D88** (2013) 114505, [arXiv:1304.1277 \[hep-lat\]](#).
- [40] N. Brambilla, S. Eidelman, P. Foka, S. Gardner, A. Kronfeld, *et al.*, “QCD and Strongly Coupled Gauge Theories: Challenges and Perspectives,” *EJPC* **74** (2014) Issue 10, [arXiv:1404.3723 \[hep-ph\]](#).
- [41] R. Höllwieser, M. Faber, Th. Schweigler, and U.M. Heller, “Chiral Symmetry Breaking from Center Vortices,” *PoS LAT2013* (2014) 505, [arXiv:1410.2333 \[hep-lat\]](#).
- [42] D. Trewartha, W. Kamleh, and D. Leinweber, “Centre Vortex Effects on the Overlap Quark Propagator,” *PoS LATTICE2014* (2014) 357, [arXiv:1411.0766 \[hep-lat\]](#).
- [43] D. Trewartha, W. Kamleh, and D. Leinweber, “Evidence that centre vortices underpin dynamical chiral symmetry breaking in SU(3) gauge theory,” *Phys. Lett.* **B747** (2015) 373–377, [arXiv:1502.06753 \[hep-lat\]](#).
- [44] M. Quandt, H. Reinhardt, and M. Engelhardt, “Center vortex model for the infrared sector of SU(3) Yang-Mills theory - vortex free energy,” *Phys.Rev.* **D71** (2005) 054026, [arXiv:hep-lat/0412033 \[hep-lat\]](#).
- [45] M. Engelhardt, “Center vortex model for the infrared sector of SU(3) Yang-Mills theory - baryonic potential,” *Phys. Rev. D* **70** (2004) 074004, [arXiv:0406022 \[hep-lat\]](#).
- [46] M. Engelhardt, “Center vortex model for the infrared sector of SU(4) Yang-Mills theory: String tensions and deconfinement transition,” *Phys. Rev. D* **73** (2006) 034015, [arXiv:0512015 \[hep-lat\]](#).
- [47] M. Engelhardt and B. Sperisen, “Center vortex model for Sp(2) Yang-Mills theory,” *Phys.Rev.* **D74** (2006) 125011, [arXiv:hep-lat/0610074 \[hep-lat\]](#).
- [48] C. Baillie, D. Johnston, and R. Williams, “Computational aspects of simulating dynamically triangulated random surfaces,” *Comp. Phys. Commun.* **58** no. 1, (1990) 105.
<http://www.sciencedirect.com/science/article/pii/001046559090139R>.
- [49] S. Catterall, “Simulations of dynamically triangulated gravity – an algorithm for arbitrary dimension,” *Comp. Phys. Commun.* **87** no. 3, (June, 1995) 409–415.
<http://www.sciencedirect.com/science/article/pii/001046559400117K>.
- [50] S. Jain and S. D. Mathur, “World-sheet geometry and baby universes in 2-D quantum gravity,” *Phys. Lett.* **B286** (1992) 239–246, [arXiv:hep-th/9204017 \[hep-th\]](#).
- [51] J. Ambjørn, S. Jain, and G. Thorleifsson, “Baby universes in 2-d quantum gravity,” *Phys. Lett.* **B307** (1993) 34–39, [arXiv:hep-th/9303149 \[hep-th\]](#).
- [52] G. Thorleifsson and S. Catterall, “A real space renormalization group for random surfaces,” *Nucl. Phys.* **B461** (1996) 350–370, [arXiv:hep-lat/9510003 \[hep-lat\]](#).
- [53] J. Ambjørn and J. Jurkiewicz, “Scaling in four-dimensional quantum gravity,” *Nucl. Phys.* **B451** (1995) 643–676, [arXiv:hep-th/9503006 \[hep-th\]](#).